HHS Public Access

Author manuscript

Proc SPIE Int Soc Opt Eng. Author manuscript; available in PMC 2019 April 08.

Published in final edited form as:

Proc SPIE Int Soc Opt Eng. 2019 February ; 10949: . doi:10.1117/12.2512989.

Artificial neural network filters for enhancing 3D optical microscopy images of neurites

Shih-Luen Wang, **Seyed M. M. Kahaki**, and **Armen Stepanyants***

Department of Physics and Center for Interdisciplinary Research on Complex Systems, Northeastern University, Boston, MA 02115, USA

Abstract

The ability to extract accurate morphology of labeled neurons from microscopy images is crucial for mapping brain connectivity and for understanding changes in connectivity that underlie learning and neurological disorders. There are, however, two problems, specific to optical microscopy imaging of neurons, which make accurate neuron tracing exceedingly challenging: (*i*) neurites can appear broken due to inhomogeneous labeling and (*ii*) neurites can appear fused in 3D due to limited resolution. Here, we propose and evaluate several artificial neural network (ANN) architectures and conventional image enhancement filters with the aim of alleviating both problems. We developed four image quality metrics to evaluate the effects of the proposed filters: normalized intensity in the cross-over regions between neurites, effective radius of neurites, coefficient of variation of intensity along neurites, and local background to neurite intensity ratio. Our results show that ANN-based filters, trained on optimized semi-manual traces of neurites, can significantly outperform conventional filters. In particular, U-Net based filtering can virtually eliminate background intensity, while also reducing the effective radius of neurites to nearly 1 voxel. In addition, this filter significantly decreases intensity in the cross-over regions between neurites and reduces fluctuations of intensity on neurites' centerlines. These results suggest that including an ANN-based filtering step, which does not require substantial extra time or computing power, can be beneficial for automated neuron tracing projects.

Keywords

image processing; image segmentation; image stack; automated neuron tracing; deep learning; machine learning

1. INTRODUCTION

Recent advances in genetic engineering and optical microscopy have allowed neuroscientists to label sparse populations of neurons and image their arbors in 3D on the scale of the entire brain [1]. At present, semi-manual tracing is the only reliable way of extracting information about the layout of axonal and dendritic branches of individual neurons from such imaging data. However, semi-manual tracing methods are very time-consuming and are prone to errors and user biases. Therefore, they are unsuitable for high-throughput neuron tracing

* a.stepanyants@neu.edu; (617)373-2944; http://www.northeastern.edu/neurogeometry/.

projects. Insufficient image quality is the main obstacle on the way to accurate automated neuron tracing [2–4]. Deep learning based methods have recently attracted great attention as a potential solution to this problem [5–7]. In particular, Li et al. [5] applied convolutional neural networks to enhance optical microscopic images of neurons prior to automated tracing, which led to a higher tracing accuracy.

Here, we consider artificial neural network (ANN) based image enhancement filters, and evaluate their performance by introducing four metrics focused specifically on features important for accurate tracing. We use two distinct datasets of images to show that ANN-based filters enhance image quality and outperform conventional filters.

2. METHODS

We evaluated the effects of three ANN-based filters (Figure 1) and three conventional filters on the quality of neuron images. The first ANN-based filter is a shallow dense network with 1 hidden layer of 100 sigmoid units. It receives an input in the form of a 21×21×7 voxel sub-image and produces a single output that represents the enhanced intensity of the central voxel. The second network is a multilayer dense network with 3 hidden layers containing 100, 50, and 100 rectified linear units (ReLU) and sigmoid units in the output layer. It receives a 28×28×10 voxel sub-image as an input and produces an output in the form of an 8×8×4 voxel sub-image. The third network is a U-Net [8, 9] with a 32×32×8 voxel input and output. It includes two dropout layers with dropout rates of 20%.

All three neural networks were trained to minimize the binary cross-entropy loss function:

$$H(y,\hat{y}) = -\frac{1}{N}\sum_{i=1}^{N}\left[y_i \log(\hat{y}_i) + (1-y_i)\log(1-\hat{y}_i)\right] \quad (1)$$

In this expression, N denotes the total number of voxels in the output, y_i is the label of voxel i, and y_i is the output value for that voxel. Adam optimizer [10] with a learning rate of 1 and a mini-batch size of 5 was used for training. To create the label, neurites in the images were semi-manually traced in 3D and optimized in the NCTracer software [11, 12] (see e.g. Figure 2A). Voxels that are less than one voxel size away from the optimized trace were labeled as 1, one voxel size away as 0.5, and greater than one voxel size away as 0 (Figure 2B). Training examples were augmented 8-fold by using image reflection and rotations by 90°, 180° and 270° in the imaging plane.

Conventional 3D filters used in this study include the Laplacian of Gaussian (LoG) filter of NCTracer (size is 2×2×2 voxels), the median filter of NCTracer (size is 3×3×3 voxels), and the MeanShift filter of ImageJ (spatial radius is 3 and color distance is 25). Parameters of conventional filters were tuned to the best of our ability to maximize image quality, and the resulting filter sizes roughly match the typical width of neurites in the images.

All filters were tested on the datasets of Neocortical Layer 1 Axons [13] and Olfactory Projection Fibers [14] used in the DIADEM challenge [15]. The first dataset includes 6

stacks of two-photon microscopy images of fluorescently labeled axons from layer 1 of mouse barrel cortex (Figure 3). The image stacks consist of 33–60 planes, each of which is 512×512 voxels in size. The second dataset includes 9 stacks of confocal microscopy images containing single axons of Drosophila olfactory projection neurons (Figure 4). These image stacks consist of 60–101 planes, each of which is 512×512 voxels in size.

ANN-based filters described in this study are available at https://github.com/neurogeometry/NNfilters.

3. RESULTS

Figure 3 shows the maximum intensity projection of one of the image stacks from the dataset of Neocortical Layer 1 Axons, along with the outputs of the three ANN-based and three conventional filters.

This dataset contains axons of multiple neurons, which presents a major challenge for automated tracing algorithms, because, in addition to tracing axons, branches belonging to different neurons must be separated into distinct trees. The latter problem is hindered by the relatively large density of axons, which appear fused in various locations due to the limited resolution of light microscopy. All filters, with the exception of MeanShift, appear to reduce the background intensity in the images. However, in contrast to the ANN-based filters, conventional filters do little to enhance the intensity of dim axons or to reduce their thickness (radius).

Figure 4 shows similar results for the dataset of Olfactory Projection Fibers. A notable feature of this dataset is that most image stacks contain axons of single neurons, intensities of which are saturated (e.g. Figure 4A). Intensity saturation increases the apparent thickness of axonal branches, which, as a result, fuse in 3D and form loops. ANN-based filters, and U-net in particular, seem to reduce axon radius, while also enhancing the intensity of very dim branches. Conventional filters, on the other hand, do not noticeably improve the images in this dataset.

We note that inferring image quality by simply viewing the images is difficult and can be misleading. Clearly, quantitative metrics are required to assess different aspects of information contained in the images. Conventional metrics, such as precision and recall, are not well suited for this task, because such measures treat image voxels independently, without regard for their correlations. Therefore, we developed four new metrics, which, in our opinion, capture morphological features that are essential for neuron tracing. The first metric reflects the intensity in the cross-over regions formed by adjacent branches. Such branches are often interconnected by tracing algorithms, and, therefore, having low intensity in the cross-over regions is favorable for tracing. Specifically, this metric is defined as the ratio of the average intensity along the brightest path (determined with A* algorithm [16]) connecting the closest points on the branches to the average intensity of the two branches in the vicinity of the cross-over (see Figure 4A inset and legend for details). The second metric is designed to reflect inhomogeneity of intensity along neurites. It is defined as the coefficient of variation (CV) of intensity along the centerlines of the lowest 10% intensity

branches. Because abrupt changes in intensity can lead to broken neuron traces, having low CVs is advantageous for tracing. The remaining two metrics are the mean effective neurite radius (measured in the NCTracer software) and the intensity ratio of local background to foreground (defined by the label).

There are trade-offs among the introduced image quality metrics. For example, one can reduce the mean effective neurite radius by means of skeletonization. This, however, can fracture dim neurites, increasing the CV of intensity along their centerlines. One can also reduce the CV of intensity of dim branches by saturating the image, but this may increase the mean effective neurite radius. Therefore, the four metrics must be considered jointly to be informative about image enhancements relevant for automated tracing.

Figure 5 shows the four image quality metrics calculated based on the original and filtered images from the datasets of Neocortical Layer 1 Axons and Olfactory Projection Fibers. According to these metrics, ANN-based filters generally outperform conventional filters. In particular, U-Net decrease intensity in the cross-over regions between neurites by more than 25% (Figure 5A 1 and 2), reduces the mean effective radius of neurites by more than 25%, to nearly 1 voxel (Figure 5B 1 and 2), and virtually eliminates background intensity (Figure 5D 1 and 2). In addition, U-Net based filter slightly enhances the intensity of dim neurites, as judged by the CV of intensity along their centerlines.

4. CONCLUSION

We showed that ANN-based filters can be successfully used to enhance morphological features of neurites in 3D optical microscopy images. These filters were applied to different datasets and produced robust reduction in normalized intensity in the cross-over regions between neurites, neurite thickness, and background intensity. U-Net, in particular, outperforms conventional image processing filters in terms of the four image quality metrics introduced in this study. The image quality metrics can also be used to assess the appropriateness of different neuron labeling and imaging methods for neuron tracing applications, including circuit mapping and structural plasticity studies. It remains to be seen if the enhancements observed in the filtered images will be reflected in the accuracy of automated neuron traces.

ACKNOWLEDGMENTS

We thank Rohan Gala for helpful discussions. This work was supported by the NIH grant R01 NS091421.

REFERENCES

[1]. Economo MN, Clack NG, Lavis LD et al., “A platform for brain-wide imaging and reconstruction of individual neurons,” Elife, 5, e10566 (2016). [PubMed: 26796534]

[2]. Acciai L, Soda P, and Iannello G, “Automated neuron tracing methods: an updated account,” Neuroinformatics, 14(4), 353–67 (2016). [PubMed: 27447185]

[3]. Meijering E, “Neuron tracing in perspective,” Cytometry A, 77(7), 693–704 (2010). [PubMed: 20583273]

[4]. Halavi M, Hamilton KA, Parekh R et al., “Digital reconstructions of neuronal morphology: three decades of research trends,” Frontiers in Neuroscience, 6, 49 (2012). [PubMed: 22536169]

[5]. Li R, Zeng T, Peng H et al., "Deep learning segmentation of optical microscopy images improves 3-D neuron reconstruction," IEEE Transactions on Medical Imaging, 36(7), 1533–1541 (2017). [PubMed: 28287966]

[6]. Turaga SC, Murray JF, Jain V et al., "Convolutional networks can learn to generate affinity graphs for image segmentation," Neural Computation, 22(2), 511–38 (2010). [PubMed: 19922289]

[7]. Januszewski M, Kornfeld J, Li PH et al., "High-precision automated reconstruction of neurons with flood-filling networks," Nature Methods, 15(8), 605–610 (2018). [PubMed: 30013046]

[8]. Çiçek Ö, Abdulkadir A, Lienkamp SS et al., "3D U-Net: learning dense volumetric segmentation from sparse annotation," International Conference on Medical Image Computing and Computer-Assisted Intervention, 424–432 (2016).

[9]. Ronneberger O, Fischer P, and Brox T, "U-Net: convolutional networks for biomedical image segmentation," International Conference on Medical Image Computing and Computer-Assisted Intervention, 234–241 (2015).

[10]. Kingma DP, and Ba J, "Adam: a method for stochastic optimization," arXiv preprint arXiv: 1412.6980, (2014).

[11]. Gala R, Chapeton J, Jitesh J et al., "Active learning of neuron morphology for accurate automated tracing of neurites," Frontiers in Neuroanatomy, 8, (2014).

[12]. Chothani P, Mehta V, and Stepanyants A, "Automated tracing of neurites from light microscopy stacks of images," Neuroinformatics, 9(2–3), 263–78 (2011). [PubMed: 21562803]

[13]. De Paola V, Holtmaat A, Knott G et al., "Cell type-specific structural plasticity of axonal branches and boutons in the adult neocortex," Neuron, 49(6), 861–75 (2006). [PubMed: 16543134]

[14]. Jefferis GS, Potter CJ, Chan AM et al., "Comprehensive maps of Drosophila higher olfactory centers: spatially segregated fruit and pheromone representation," Cell, 128(6), 1187–1203 (2007). [PubMed: 17382886]

[15]. Brown KM, Barrionuevo G, Canty AJ et al., "The DIADEM data sets: representative light microscopy images of neuronal morphology to advance automation of digital reconstructions," Neuroinformatics, (2011).

[16]. Hart PE, Nilsson NJ, and Raphael B, "A formal basis for the heuristic determination of minimum cost paths," IEEE Transactions on Systems Science and Cybernetics, 4(2), 100–107 (1968).

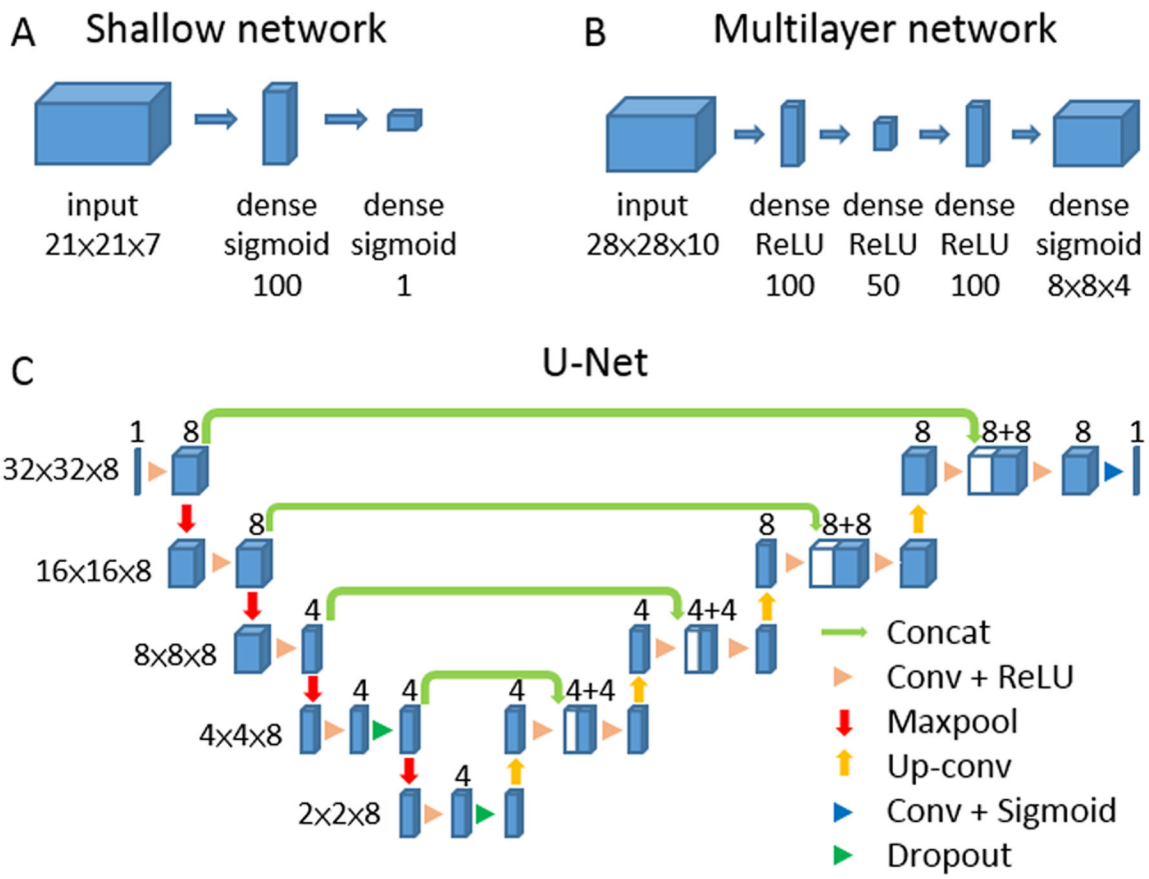

Figure 1.

Architectures of 3D ANN-based filters used in this study. A. Shallow feedforward network with dense connectivity and sigmoidal neurons. Blue boxes represent neuron layers with neuron numbers shown. The network receives a 21×21×7 voxel sub-image as an input and generates a scalar output. B. Multilayer feedforward network with dense connectivity and ReLU neurons. This network has a bottleneck. It receives a 28×28×10 voxel sub-image as an input and generates an 8×8×4 voxel output. C. U-Net. Blue boxes represent feature maps with the number of channels denoted above each box. The network receives a 32×32×8 voxel input and generates an output of the same size.

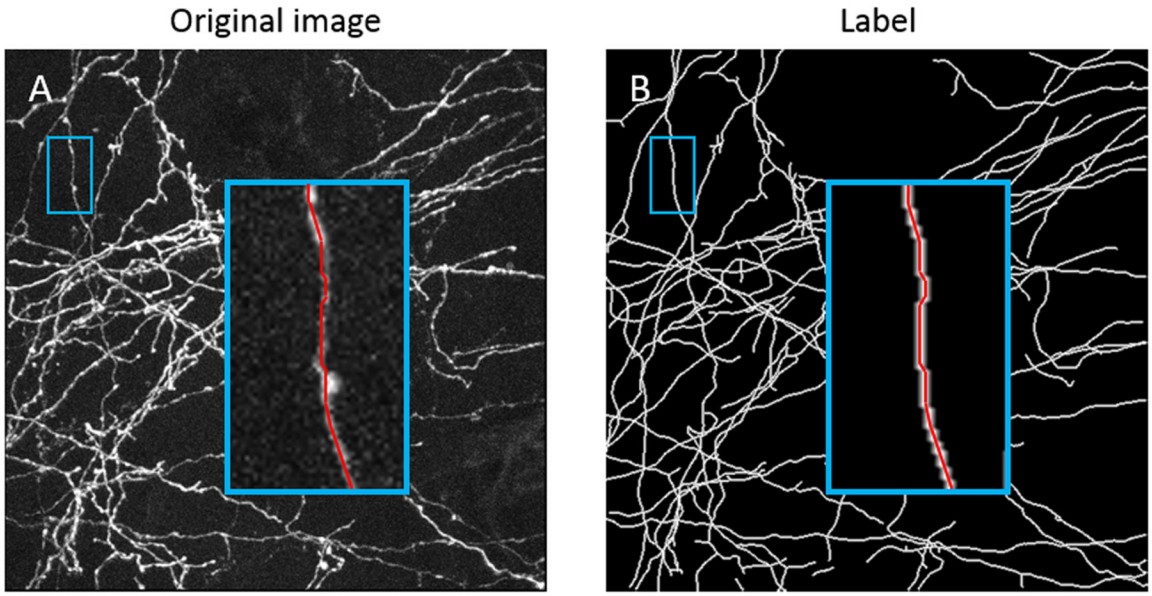

Figure 2.

Creating a label from an intensity image. A. Maximum intensity projection of an image stack containing layer 1 axons of mouse neocortical neurons. All axons were traced semi-manual and optimized in the NCTracer software. The inset shows a zoomed-in view of an axon segment. Red line is the optimized trace of the axon centerline. B. Maximum intensity projection of the labeled stack corresponding to (A). Voxels located less than one voxel size away from the trace are labeled as 1 (white), exactly one voxel size away as 0.5 (gray), and greater than one voxel size away as 0 (black). The widths of the blue rectangles correspond to 14 μm.

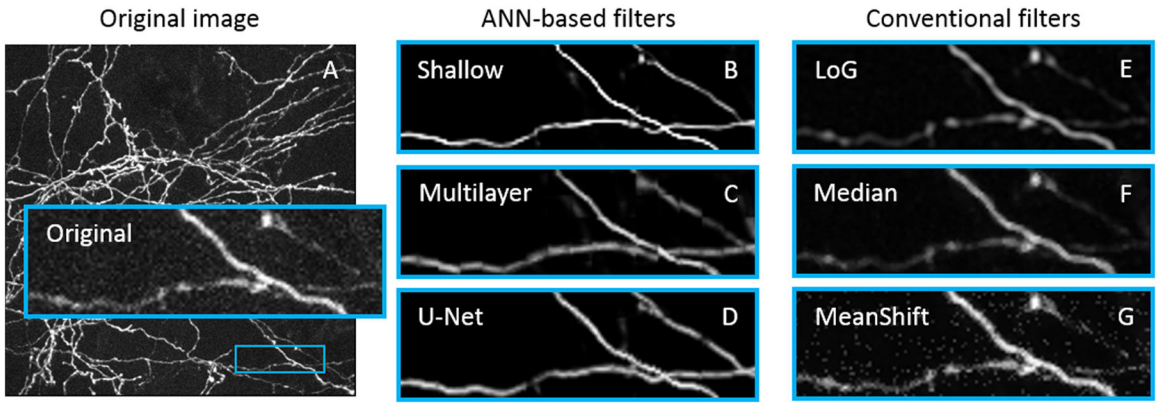

Figure 3.

Images of Neocortical Layer 1 Axons enhanced with the proposed and conventional image processing filters. A. Maximum intensity projection of an image stack. The inset shows a 4× zoomed-in view of a small region outlined with the blue rectangle. B-G. The same region in the images enhanced with ANN (B-D) and conventional filters (E-G). The widths of the blue rectangles correspond to 40 μm.

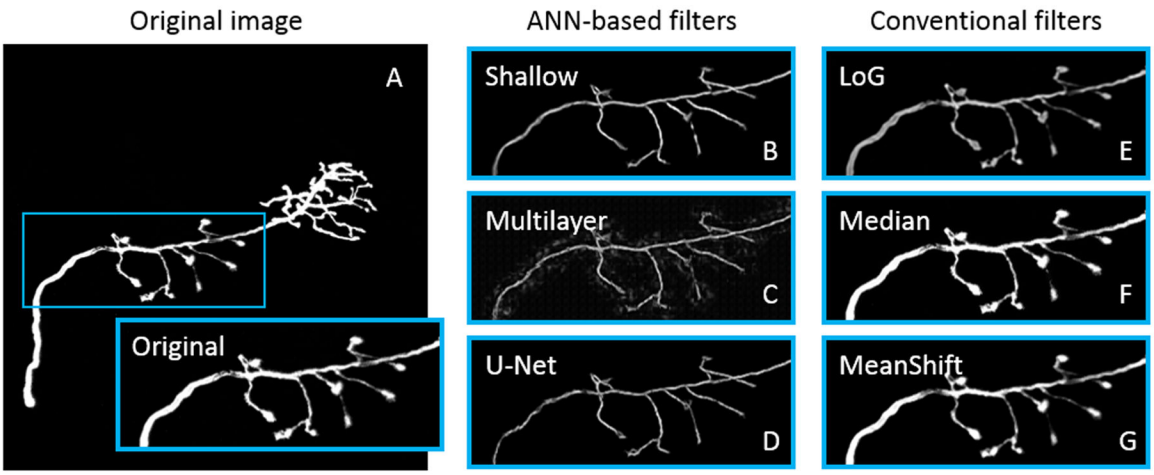

Figure 4.

Images of Olfactory Projection Fibers enhanced with the proposed and conventional image processing filters. A. Maximum intensity projection of an image stack. The inset shows a zoomed-in view of a region outlined with the blue rectangle. B-G. The same region in the images enhanced with ANN (B-D) and conventional filters (E-G). The widths of the blue rectangles correspond to 85 μm.

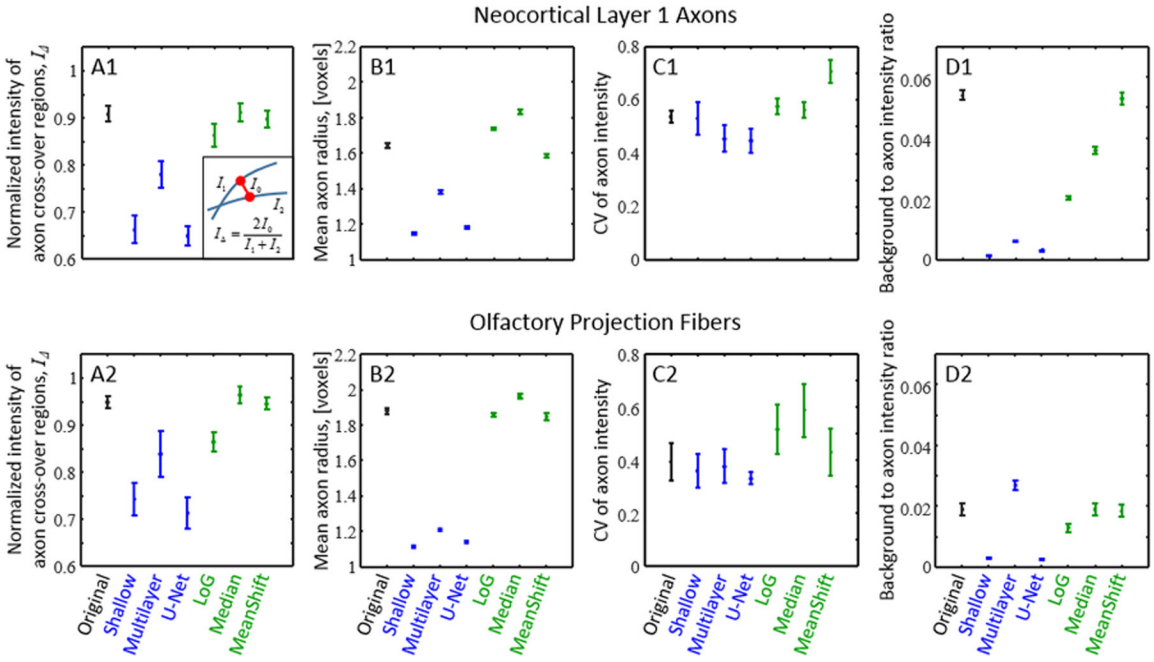

Figure 5.

Quality of images enhanced with the ANN (blue error bars) and conventional (green error bars) filters for the datasets of Neocortical Layer 1 Axons (top row) and Olfactory Projection Fibers (bottom row). A. Normalized intensity in the cross-over regions between axons. The inset illustrates how this metric is calculated. Cross-over is defined as a location in the image stack where two axon branches come within 10 voxels of each other. I_1 and I_2 denote the average intensities of A* paths along the axons in the vicinity (within 5 voxels) of the cross-over. I_0 is the average intensity of the A* path connecting the two closest points on the axons (red line). B. Effective axon radius calculated for the A* axon centerline voxels. C. Coefficient of variation of intensity along the A* axon centerlines calculated for the 10% of lowest intensity branches. D. Local background to foreground intensity ratio. Local intensities are based on randomly sampled 64×64×10 sub-images, in which background and foreground voxels are defined by the label. Error bars correspond to s.e.m.